The fate of hippocampal synapses depends on the sequence of plasticity-inducing events

J. Simon Wiegert[1,2], Mauro Pulin[1,2], Christine E. Gee[1], and Thomas G. Oertner[1]*

[1] Institute for Synaptic Physiology, Center for Molecular Neurobiology Hamburg (ZMNH), 20251 Hamburg, Germany

[2]Research Group Synaptic Wiring and Information Processing, Center for Molecular Neurobiology Hamburg (ZMNH), 20251 Hamburg, Germany

*Correspondence: thomas.oertner@zmnh.uni-hamburg.de

Abstract

The hippocampus is able to store information about salient external events for several weeks. Synaptic weight adjustments, expressed as long-term potentiation (LTP) and depression (LTD) of synaptic transmission, are thought to be essential for the formation of episodic memories. Previous studies have shown that LTP and LTD respectively increase and decrease the lifetime of individual hippocampal synapses, suggesting that initially graded weight adjustments may be consolidated in the form of an altered connectivity matrix. However, during their lifetime, synapses may undergo multiple weight adjustments, and it is not known how sequential potentiation and depression events are integrated at individual synapses. Here we use optogenetic 5 Hz ("theta frequency") stimulation to induce LTP and 1 Hz ("low frequency") stimulation to induce LTD at identified synapses. Synaptic potentiation was NMDA receptor-dependent and contingent on complex spike bursts in the postsynaptic neurons. Potentiated synapses typically persisted for the next 7 days whereas spines in their vicinity were destabilized, suggesting highly specific regulation of synaptic lifetime by a 'center-surround' contrast mechanism. When successful, induction of LTD the day after LTP reversed the stabilizing effect of LTP. Vice versa, LTP induction overwrote the destabilizing effect of LTD. We conclude that multiple weight adjustments are not summed in a linear fashion, but the most recent plasticity event determines the lifetime of a Schaffer collateral synapse.

Introduction

Graded changes in synaptic strength, driven by specific activity patterns, are a candidate mechanism for information storage in the brain (1). When entire pathways are potentiated by high frequency stimulation, the increase in synaptic coupling can indeed be recorded for several days (2). Increases in the size of synapses, the number of postsynaptic transmitter receptors and release of transmitter, have been shown to underlie increases in synaptic strength. A prevailing theory is that graded changes in synaptic strength persist as a memory trace of former activity. At the level of individual synapses, however, dramatic fluctuations in spine volume over time scales of hours to days, cast doubt on whether information can be stored for long periods in the analog strength of synapses (3, 4). An alternative hypothesis is that over longer time periods,

information is stored not in the strength but in the number of connections, which, at the level of individual synapses, would manifest as a change in synaptic lifetime. Supporting evidence comes from the findings that long term depression (LTD) decreases synaptic lifetime (5–7) and that spine structure becomes stabilized and growth persists up to 3 days after induction of long term potentiation (LTP) (8, 9).

An important consideration is that new information, manifest as changing patterns of activity, constantly arrives at synapses. How a synapse that has once undergone LTP responds when a normally LTD inducing pattern of activity arrives one day later and vice versa has been almost entirely unstudied. Shortly after LTP induction, it is possible to depotentiate synapses, but this is a phenomenon that may occur only 1-2 hours after LTP induction (10–12). Our goals were to monitor the fate of individual spine synapses after induction of LTP and to explore how sequential plasticity-inducing events affect synaptic lifetime. Are spine synapses able to integrate multiple plasticity events over time, or does either the first or last form of plasticity determine their lifetime? Using organotypic hippocampal slice cultures and optical stimulation of channelrhodopsin-expressing CA3 pyramidal neurons, we found that Schaffer collateral synapses could be potentiated by 5 Hz stimulation if complex spike bursts were induced in the postsynaptic CA1 neuron (13). We then followed the fate of the identified synapses over 7 days.

As suggested by previous studies, LTD and LTP differentially affected synaptic lifetime. What was not expected is that sequentially inducing LTD and LTP did not return spines to their basal state, but the spine lifetime matched that of spines which only underwent LTP. Once LTP was induced, it became almost impossible to induce subsequent LTD. In the few experiments were LTD could be induced 24 h after LTP, synaptic lifetime was similar to that of spines that only underwent LTD. Thus, multiple weight adjustments are not summed in a linear fashion, but the most recent plasticity event determines the lifetime of a Schaffer collateral synapse.

Results

Optical theta frequency stimulation induced LTP at Schaffer collateral synapses. CA3 neurons expressing the light-sensitive channel ChR2(E123T/T159C) (14) together with the presynaptic vesicle marker synaptophysin-tdimer2 were stimulated with short pulses of blue light (2 ms

long, 40 ms interval, λ = 470 nm). On CA1 pyramidal cells expressing GCaMP6s and mCerulean, active spines were identified by imaging stimulation-induced excitatory postsynaptic calcium transients (EPSCaTs). After an active spine was identified we switched to line scanning mode, defining a scan curve that intersected the responding spine and a small number of neighboring spines at high speed (500 Hz, Fig. 1A). Calcium transients were restricted to the responding spine and were not detected in the dendrite. A neighboring CA1 cell ('reporter neuron') was patch-clamped to simultaneously record excitatory postsynaptic synaptic currents (EPSCs). Light stimulation evoked EPSCs with a magnitude of 1330 ± 220 pA, consistent with our previous study (6). To induce LTP, we stimulated CA3 pyramidal cells with 150 light pulses at 5 Hz, a theta-frequency stimulation (TFS) paradigm, which potentiates CA3-CA1 but not CA3-CA3 synapses in an NMDAR-dependent fashion (13, 15). TFS-induced LTP requires transient (30 s) stimulation of enough CA3 cells to drive postsynaptic CA1 cells to fire complex spike bursts (CSBs, fig. S1) (13). We adjusted the stimulation light intensity to recruit more and more CA3 neurons until the synaptic drive was just below the action potential threshold in the CA1 reporter neuron. During optogenetic theta-frequency stimulation (oTFS), the reporter neuron responses changed from mostly subthreshold EPSPs with occasional single action potentials to CSBs (Fig 1C, fig. S1) (16). CSBs in the reporter neuron were time-locked with large calcium transients in the stretch of dendrite adjacent to the postsynaptic spine (Fig 1B, middle column), suggesting that synchronized CSBs were occurring in neighboring neurons. EPSCaTs were strongly potentiated 30 min after oTFS, generating calcium transients that frequently spread into the dendrite (Fig. 1B, Fig. 2B). Likewise, the amplitude of EPSCs in the reporter neuron increased after oTFS, indicating successful induction of LTP (Fig. 1B, Fig 2A). Both CSBs and LTP induction were blocked in the presence of the NMDA receptor antagonist APV (Fig 2A and B). Thus, oTFS was dependent on NMDAR activation as previously demonstrated (13). In some experiments, CSBs and large dendritic calcium transients did not occur during oTFS, likely due to an insufficient number of virus-transfected CA3 pyramidal neurons. When no large dendritic calcium transients were triggered during oTFS, spine calcium signals were not consistently potentiated 30 min after oTFS (Fig. 2B, Fig. S2*A, B*).

Taking into consideration only those experiments in which CSBs and dendritic calcium transients were evoked during oTFS, we observed that neither the amplitude nor the potency (amplitude of successes) of EPSCaTs changed immediately after oTFS. Thirty minutes later, however, both were significantly increased (Fig. 2C). The slowly developing potentiation was also reflected in the EPSCs recorded in the reporter neuron (Fig. 2A), consistent with previous reports (13, 15). LTP had no significant effect on the probability of EPSCaT occurrence (P_{Ca}, fig. 2C), suggesting that the potentiation was mainly due to postsynaptic changes. Interestingly, while EPSCaT potency was not affected in experiments where no CSBs were elicited during oTFS, P_{Ca} was significantly reduced (Fig. S2*C*). Thus, in experiments where the synaptic drive was not strong enough to trigger postsynaptic spikes, presynaptic activity in the theta frequency range appeared to elicit a weak form of presynaptic depression.

Optogenetic TFS-induced synaptic potentiation was accompanied by slow changes in spine structure (mCerulean, fig. 2D). The head volume of spines that experienced CSBs was unchanged immediately after oTFS, but increased by 21 ± 6% during the next 30 min. The nearest neighboring spines also showed a small but significant increase in volume (15 ± 3%), whereas no consistent change was detected at more distant spines (2 ± 3%). When oTFS failed to elicit CSBs or when NMDA receptors were blocked during oTFS, stimulated spines did not exhibit significant volume changes (Fig. S2*D, E*).

We next asked whether synaptic potentiation was maintained during the 24 hours following oTFS. Consistent with our first data set, spine head volume and EPSCaT potency were significantly increased 30 min after oTFS (Fig. 3A and B). Twenty-four hours after LTP induction, however, both measures had returned to baseline. We detected no significant change in EPSCaT probability either 30 min or 24 hours after oTFS (Fig. 3C). Thus, beyond the acute effects on the day of potentiation, we did not observe permanent changes in synaptic strength after oTFS-induced LTP.

Effect of long-term potentiation on synaptic lifetime. Next, we determined whether oTFS-induced LTP affected synaptic lifetime. Previous work showed that potentiated spines are not characterized by permanently enlarged heads, but are less likely to be eliminated during the

next 3 days (8). We therefore assessed the stability of potentiated spines and their neighbors during the following week. Under control conditions without external stimulation, 27% of all spines disappeared between days 1 and 7. This turnover rate is in agreement with previous measurements in hippocampal slice cultures (6) and in mice *in vivo* (17). LTP induced by oTFS appeared to increase synaptic lifetime, as between days 1 and 7, only 1 out of 14 potentiated spines disappeared (Fig. 3D and E). The stability of spines next to the potentiated spine was also affected, mirroring the transient head volume changes on day 0 (Fig. 2D and 3A). Compared to controls, nearest-neighbor spines disappeared less often between days 1 and 7 whereas more distant spines (> 5 µm) were eliminated more often (Fig 3E). These findings suggest that biochemical signals activated by oTFS spread locally from the activated synapse to neighboring spines (18), affecting acutely their size and on longer timer scales, their survival.

Effects of sequential plasticity-inducing protocols on synaptic lifetime. As we established previously, optogenetic low frequency stimulation (oLFS, 900 APs at 1Hz) induces long-term depression (LTD) at Schaffer collateral synapses (6). In agreement with our previous results, 45% of spines that received oLFS disappeared between days 1 and 7 (Fig. 4A). LTD induced by oLFS is associated with presynaptic depression which may reduce the activity of the synapse in the days following plasticity induction. If the frequency of synaptic activity is a crucial factor determining synaptic lifetime, increasing synaptic activity might suffice to rescue doomed synapses. To test this hypothesis, we induced LTD on day 0 by oLFS. Starting 30 min after oLFS, we continued stimulating the CA3 neurons in the incubator every 10 sec until day 7. Indeed, this chronic activation protocol rescued the doomed spines, as only in 1 out of 9 experiments (11%) the LTD'ed spine disappeared before day 7 (Fig. 4B). The spine loss probability was less than that seen for control spines (27%, Fig 3E) and close to that seen after LTP (7%).

Since enhanced synaptic transmission reverted LTD-triggered synapse elimination, we speculated that if LTP were induced after LTD, the doomed spines would also be stabilized. We tested this by inducing LTP 24 h after LTD induction. LTD was considered successful when the average spine Ca^{2+} response dropped to less than 90% of the baseline response 30 min after oLFS, which was the case in 70% (28/40) of the experiments (Fig. 4D). Twenty-four hours later, we applied oTFS to the spines that were depressed on the previous day. LTP induction was

considered successful when the average spine Ca^{2+} response increased to more than 110% of the baseline response after TFS, which was the case in 64% (18/28) of all experiments on day1. Thus, we considered synapses that either underwent LTD followed by LTP (45% of all tested synapses) or only LTD (when LTP induction was not successful; 25% of all tested synapses). Synapses that did not display LTD after oLFS (30% of all tested synapses) were not considered further. When LTP was induced after LTD, only 12% of spines disappeared between days 1 and 7, indicating stabilization of doomed synapses. Of the spines that received oTFS after LTD but did not get potentiated, 43% disappeared between days 1 and 7, similar to the 45% disappearance rate seen after oLFS only (Fig. 4A, D). Thus, EPSCaT amplitudes measured 30 min after the second round of plasticity induction were predictive of spine survival assessed 6 days later.

We next tested whether the LTP-induced stabilization of spines would persist even if LTD were subsequently induced (Fig. 5A). LTP on day 0 was induced in 72% (18/25) of spines after oTFS (Fig. 5B), similar to the set of oTFS experiments 1 day after oLFS (64%, $p = 0.85$) and the first set of oTFS experiments (Fig. 2B 62%, 26/42, $p = 0.41$). Again, we considered only those spines where LTP was successfully induced during the following days. When oLFS was applied 24 h later, we observed that LTD was induced in only 33% (6/18) of previously potentiated spines on the next day (Fig. 5B), a much poorer success rate than the 70% when oLFS was applied with no prior plasticity. Interestingly, in experiments where LTD could not be induced, we observed action potentials during oLFS in the reporter neuron more frequently than when LTD induction was successful (median # of APs: 0.5 vs. 85.0), suggesting increased excitability of the culture one day after oTFS. In the few experiments were LTD was successfully induced 24 h after LTP, 50% of spines disappeared by day 7 (Fig. 5B). In the more typical case where oLFS failed to induce LTD, only 8% of spines disappeared by day 7. Thus, the stabilizing effect of LTP on spines can be overwritten by subsequent LTD (Fig. 5C), but this sequence of plasticity events is not very likely to happen.

Discussion

Theta burst stimulation (TBS, 100 Hz bursts repeated at 5 Hz) is a common experimental protocol to induce LTP *in vitro* (11). While individual CA3 pyramidal cells often fire action potentials rhythmically at 5 Hz (theta frequency range) they do not spike at high frequencies such as 100 Hz *in vivo* (19). Here we show that LTP and spine-specific stabilization can be induced at 5 Hz, the typical carrier frequency of rodent hippocampus, if a sufficient number of inputs are activated synchronously (13, 15). Theta-frequency stimulation (TFS) is the physiological equivalent of spike-timing dependent potentiation, replacing the artificial current injection into the postsynaptic neuron by highly synchronized excitatory synaptic input. Synchronized synaptic input can trigger dendritic calcium spikes, local regenerative events caused by the opening of voltage-dependent channels (NMDARs and VDCCs). These events can be electrophysiogically identified as complex spike bursts, consisting of several fast sodium spikes on top of a broader depolarization mediated by dendritic calcium currents (16, 20–22). In our experiments, the occurrence of dendritic calcium spikes during the induction protocol was highly predictive of successful LTP induction at individual synapses (Fig. 2B). Recent studies in head-fixed mice running on a treadmill suggest that theta-frequency modulated synaptic input to CA1 pyramidal cells triggers dendritic calcium spikes which are required for synaptic potentiation and place cell formation (23, 24). Thus, dendritic calcium spikes during complex spike bursts, evoked by synchronized input from entorhinal cortex and CA3 pyramidal cells, are part of the physiological mechanism for the selective potentiation of active Schaffer collateral synapses during behavior (25).

Spine calcium imaging allowed us to distinguish between presynaptic changes, affecting the probability of EPSCaT observation after presynaptic stimulation (P_{Ca}), and postsynaptic changes, affecting the amplitude of successful EPSCaTs ('potency'). Even though newly inserted AMPA receptors may not be permeable for calcium themselves, stronger depolarization of the spine head during the EPSP leads to more efficient unblocking of NMDA receptors and EPSCaT potentiation, albeit in a non-linear fashion that depends on the resistance of the spine neck (26). In contrast to LTD, where the reduction in average EPSCaT amplitude was mainly due to an increase in the synaptic failure rate (6), oTFS-induced LTP strongly enhanced EPSCaT potency,

but did not seem to affect release probability. This confirms that postsynaptic mechanisms such as AMPA receptor insertion account for this form of potentiation (27–29). Analyzing spine volume changes supported the notion of differentially localized plasticity mechanisms: While LTD induction did not affect spine volume (6), LTP triggered significant growth of the postsynaptic compartment (Fig. 2D). Going beyond the first hours after plasticity induction, we asked how these different forms of plasticity would influence the tenacity of synapses that actively contributed to postsynaptic spiking in comparison to inactive synapses on the same dendrite.

Twenty-four hours after induction of LTP, synapses were back to their baseline state with respect to the amplitude and probability of spine calcium transients as well as the volume of the spine head. Yet, a long-lasting, synapse-specific memory of the potentiation event was maintained, since these once-potentiated spines were more likely to persist during the following week compared to other spines on the same dendritic branch, or non-stimulated controls. For LTD, similar results were reported: Spines did not show any lasting decrease in volume, but their life expectancy was significantly reduced (6). This supports the theoretical concept that information could be robustly stored in the topology of the network rather than in the analog strength of individual synapses. The mechanism linking LTP to synaptic stabilization, and LTD to destabilization, is likely to involve several processes. Synaptic tenacity is known to be affected by trans-synaptic proteins such as Neuroligin-1 and SynCAM-1 (30, 31), PSD-95 (8, 32), ubiquitin protein ligase E3A (33), ensheatment of the synapse by astrocyte processes (34) and many other local factors. In addition, frequent use of a synapse might also be important for its maintenance, a notion that is supported by our chronic activation experiments (Fig. 4B). It may be a combination of local physical changes and distributed network effects, such as the frequent reactivation of a specific circuit, which makes once potentiated synapses robust against depression (Fig. 5B) and pruning (Fig. 3E). The link between LTP and long-term structural stability we show on the single-synapse level could explain why learning-induced spines in motor cortex are more stable than their pre-existing neighbors and persist for months after training (35, 36). LTP-induced tenacity might be a general principle to connect different time scales of cortical circuit plasticity.

Optogenetic TFS not only affected the volume and long-term stability of the stimulated spine, but also increased volume and stability of is immediate neighbors (Fig. 2D). This is consistent with short-range diffusion of 'potentiating factors' such as activated RhoA and Cdc42 out of the directly stimulated spine (37, 38). In contrast, more distant spines on the same dendrite (5-10 µm) showed no increase in volume and a decrease in lifetime (Fig. 3E), confirming an earlier 3-day study (8). Since we increased the optogenetic drive to CA3 during oTFS, we could not map the position of all spines that were active during plasticity induction. Therefore, we were not able to study the spatial extent of spine destabilization, e.g. by selecting a 'control' branch that received no input during oTFS. By inducing two rounds of plasticity, we demonstrated that synaptic pruning is not a random process, but determined by the last plasticity-inducing activity pattern. In the organotypic culture system, the latency between LTD induction and spine loss was several days. This period could be considerably shorter *in vivo*, given the highly rhythmic activity of the hippocampal circuit and in consequence, intense synaptic competition. Our approach allows imposing any kind of spike pattern to a select group of synapses over several days. It complements *in vivo* studies of structural plasticity, which provide information about spine turnover, but not about the activity patterns in pre- and postsynaptic neurons (17). Once the conditions for synaptic maintenance are understood, the protracted process of circuit refinement by constant removal of irrelevant synapses could be simulated. Networks with self-organized connectivity might generate activity patterns that are different from the randomly connected networks underlying current large-scale simulations (39). Thus, together with realistic simulations of synaptic network dynamics and long-term investigations of synapse remodeling in vivo, our detailed long-term analysis of the structure-function relationship of individual synapses may help to better understand how the brain stores and retrieves memories.

Materials and Methods

Materials and methods used in this study were largely identical to those used in a previous study (6).

Slice Culture Preparation and transfection. Hippocampal slice cultures from male Wistar rats were prepared at postnatal day 4–5 as described (40). Animal procedures were in accordance with the guidelines of local authorities and Directive 2010/63/EU. At DIV 3, we pressure-injected rAAV2/7 encoding ChR2(ET/TC)-2A-synaptophysin-tdimer2 into CA3. At DIV 18, single-cell electroporation was used to transfect CA1 pyramidal neurons in rAAV-infected slices with GCaMP6s and Cerulean (ratio 1:1) as described (41).

Electrophysiology. Experiments were performed between DIV 21 and 25. Whole-cell recordings from CA1 pyramidal cells were made at 25°C with a Multiclamp 700B amplifier (Molecular Devices). Patch pipettes with a tip resistance of 3-4 MΩ were filled with (in mM) 135 K-gluconate, 4 $MgCl_2$, 4 Na_2-ATP, 0.4 Na-GTP, 10 Na_2-phosphocreatine, 3 ascorbate, and 10 HEPES (pH 7.2). LTD experiments were conducted in ACSF containing (in mM) 135 NaCl, 2.5 KCl, 4 $CaCl_2$, 4 $MgCl_2$, 10 Na-HEPES, 12.5 D-glucose, 1.25 NaH_2PO_4, 0.03 D-Serine (pH 7.4, sterile filtered). During LTP induction, ACSF with lower divalent ion concentration (2 $CaCl_2$, 1 $MgCl_2$) was used to increase excitability.

Two-Photon microscopy. The custom-built two-photon imaging setup was based on an Olympus BX51WI microscope equipped with a LUMPLFLN 60x 1.0 NA objective, controlled by the open-source software package ScanImage (42) which was modified to allow user-defined arbitrary line scans at 500 Hz. Two Ti:Sapphire lasers (MaiTai DeepSee, Spectra-Physics) controlled by electro-optic modulators (350-80, Conoptics) were used to excite cerulean (810 nm) and GCaMP6s (980 nm). To activate ChR2(ET/TC)-expressing cells outside the field of view of the objective, we used a fiber-coupled LED (200 µm fiber, NA 0.37, Mightex Systems) to deliver light pulses to CA3. During the blue light pulses, sub-stage PMTs (H7422P-40SEL, Hamamatsu) were protected by a shutter (NS45B, Uniblitz).

Measuring excitatory postsynaptic calcium transients (EPSCaTs). Frame scans (10×10 µm) of oblique dendrites were acquired to detect spines responding to optogenetic stimulation of CA3 neurons. Two brief (2 ms) light pulses with an inter-pulse interval of 40 ms were applied to increase release probability and thus the chance of detecting responding spines. In each trial, 14 frames (64×64 pixel) were acquired at 7.8 Hz. At least 5 trials were recorded from each dendritic

segment. The relative change in GCaMP6s fluorescence ($\Delta F/F_0$) was calculated on-line. If the spine signal exceeded 2 times the standard deviation (SD) of its resting fluorescence, this spine was considered as 'potentially responding'. To measure Ca^{2+} transients with better signal-to-noise ratio, line scans were acquired across potentially responding spine heads and their parent dendrites (500 Hz, 20 trials / spine). To measure the amplitude of Ca^{2+} transients and to distinguish successful synaptic transmission events (EPSCaTs) from failures, we used a template-based fitting algorithm. The characteristic fluorescence time constant was extracted for every spine by fitting a double exponential function (τ_{rise}, τ_{decay}) to the average GCaMP6s signal. To estimate the Ca^{2+} transient amplitude for every trial, we fit the spine-specific template to every response, amplitude being the only free parameter. Response amplitude was defined as the value of the fit function at its maximum. A trace was classified as 'success' when its amplitude exceeded two standard deviations (2σ) of baseline noise.

Long-term imaging of spine morphology: The use of HEPES-buffered sterile-filtered ACSF allowed us to optically stimulate and image slice cultures under near-sterile conditions, using no perfusion system. The custom recording chamber (1 mm quartz glass bottom) and 60× water-immersion objective were sterilized with 70% ethanol and filled with 1.5 ml sterile ACSF. A small patch of membrane (5 × 6 mm) supporting the hippocampal culture was cut out of the cell culture insert (Millipore PICM0RG50), placed in the recording chamber and weighted down with a u-shaped gold wire. During imaging, the temperature of the slice culture was maintained at 25°C via a permanently heated oil-immersion condenser (NA = 1.4, Olympus). After each imaging session, the membrane patch was placed on a fresh sterile membrane insert and returned to the incubator. In the first imaging session, a spine displaying stimulation-induced EPSCaTs was centered and a three-dimensional image stack (XY: 10×10 µm, Z: 5-15 µm) of the mCerulean signal was acquired. Additional image stacks were acquired at low magnification to ensure identity of the dendritic segment. For post-hoc analysis of spine turnover, the three-dimensional image stacks were aligned based on a rigid-body algorithm (ImageJ). All spines identified in the three-dimensional image stack acquired before the plasticity induction protocol were analyzed in the subsequent stacks, with the following exception: Spines that appeared shifted from their original position on the dendrite by more than 1 µm in any direction between

two consecutive imaging sessions were not included in the analysis, as it was not clear whether the original spine was replaced by a new one. Maximum intensity projections are shown for illustrative purposes only and were not used for analysis. To estimate spine volume, we integrated the fluorescence intensity of the spine head (mCerulean) taken from a single optical section through the center of the spine.

Statistics: All statistical analysis was performed using GraphPad Prism 6.0. Data were tested for Gaussian distribution by D'Agostino & Pearson omnibus normality test. Normally distributed data were tested for significant differences with a two-tailed t-test (Fig. 3A) or one-way repeated-measures analysis of variance (ANOVA) followed by Sidak's multiple comparisons test (Fig. 3B, C). Data with non-normal distribution data were tested with the following nonparametric tests: Two-tailed Wilcoxon matched-pairs signed rank test (Fig. 2A, D, 3A), Friedman test followed by Dunn's multiple comparison test (Fig. 2C, S2A-C). Investigators were not blinded to the group allocation during the experiments. Data analysis was done with unsupervised analysis software if possible to preclude investigator biases. All experiments were done with interleaved controls and treatment groups were mixed, where possible.

Acknowledgements

We thank Iris Ohmert and Sabine Graf for excellent technical assistance, Christian Schulze for modifications of ScanImage software, and Ingke Braren and the viral vector core facility of the University Medical Center Hamburg-Eppendorf for the production of rAAV. This study was supported by the Deutsche Forschungsgemeinschaft DFG through Research Unit FOR 2419 (P4 and P7), Priority Programs SPP 1665 and SPP 1926, and Collaborative Research Center SFB 936 (B7) and the European Research Council (ERC-2016-StG 714762).

Figure legends

Fig. 1. Channelrhodopsin-driven theta-frequency stimulation induces LTP. (A) Left: A fiber-coupled LED (λ = 470 nm) was used to locally stimulate ChR2-expressing CA3 neurons. Spines on GCaMP6s/cerulean-expressing CA1 pyramidal cells were imaged with two-photon microscopy. For parallel electrical recordings, a second CA1 neuron was patch-clamped (reporter neuron). Middle: oblique dendrite branching off the apical trunk filled with mCerulean. Detection of active spines was done with GCaMP6s during presynaptic optogenetic stimulation. Stimulation-induced fluorescence changes (ΔF) of GCaMP6s were analyzed in fast frame scans (squares) of oblique dendrites until a responsive spine was detected (red square). Right: Magnified view of GCaMP6s fluorescence in the dendritic section harboring an activated spine. The laser was scanned in a user-defined trajectory across multiple spines and the parental dendrite during Ca^{2+} imaging (red curve). (B) Fluorescence signal across time from arbitrary line scan on dendrite shown in A during ChR2-stimulation before (left) and after (right) optical theta-frequency stimulation (oTFS). Temporally matched traces from multiple trials and electrophysiological recording from a reporter neuron are shown below. Middle: GCaMP6s-signal at 4 selected time points during oTFS. GCaMP6s-traces from spine 1 and dendrite and electrophysiological recording from a reporter neuron are shown below.

Fig. 2. Characterization of oTFS-induced LTP. (A) Changes in excitatory postsynaptic current (EPSC) amplitude in reporter neurons immediately after and 30 min after oTFS in the absence (left) or presence (right) of the NMDA receptor antagonist APV during oTFS. EPSCs were significantly increased after 30 min ($p = 0.012$, $n = 20$ slice cultures). The increase was blocked by APV ($p = 0.69$, $n = 6$ slice cultures). (B) Relative change of average excitatory Ca^{2+} transients (EPCaTs) in individual spines 30 min after the oTFS protocol plotted against the average spine Ca^{2+} during oTFS. In experiments indicated by filled red circles, APV was present during oTFS. (C) EPSCaT amplitude ($p = 0.0008$, $n = 20$ slice cultures) and EPSCaT potency (successes only, $p = 0.0025$) but not EPSCaT probability (P_{Ca}, $p > 0.05$) were increased 30 min after oTFS in experiments where complex spike bursts (CSBs) were induced during oTFS. (D) Maximum intensity projections of mCerulean fluorescence in dendritic segment harboring a responding spine that was successfully potentiated (blue arrowhead). Right: Volume of oTFS spines (p =

0.002, n = 26 spines) and nearest (p = 0.0001, n = 45 spines) but not distant neighbors (p = 0.83, n = 58 spines) was increased 30 min after oTFS in experiments where CSBs were induced during oTFS. For details on the statistical tests, please refer to the Materials and Methods section.

Fig. 3. Long-term outcome of oTFS-induced LTP. (A) Analysis of volume changes of oTFS spines 30 min and 24 h after oTFS. The volume increase 30 min after oTFS (p = 0.03, n = 15 slice cultures) was not maintained 24 h later (p = 0.42). (B) Analysis of EPSCaT potency before, 30 min and 24 h after oTFS. The increased potency 30 min after oTFS (p = 0.015, n = 14 slice cultures) has significantly decreased again 24 h later (p = 0.005) and was similar to the condition before oTFS (p = 0.55). (C) EPSCaT probability (P_{Ca}) did not change 30 min and 24 h after oTFS (p = 0.32, n = 14 slice cultures). For details on the statistical tests, please refer to the Materials and Methods section. (D) Long-term survival analysis after LTP. Spines were imaged at d0, d1 and d7. Below: Maximum intensity projections of mCerulean fluorescence in dendritic segment harboring a responding spine that was successfully potentiated (green arrowhead). (E) Quantification of spine survival after 7 days under baseline conditions without any optical stimulation (left, black) or after successful LTP induction on day 0. Surviving fractions are shown for responding spines, nearest and distant neighbors.

Fig. 4. LTD-induced spine elimination is reversed by LTP or sustained synaptic transmission. (A) Long-term survival analysis after LTD. Spines were imaged at at d0, d1 and d7. Below: Maximum intensity projections of mCerulean fluorescence in dendritic segment harboring a responding spine that was successfully depressed (red arrowhead). Open arrowhead on day 7 indicates position of eliminated spine. Corresponding EPSCaT traces from indicated time points are shown in red. Pie chart shows quantification of spine survival after 7 days. (B) Long-term survival analysis of experiments where depressed synapses were continuously stimulated (0.1 Hz) after LTD. Below: Maximum intensity projections of mCerulean fluorescence in dendritic segment harboring a responding spine that was successfully depressed on day 0 (blue arrowhead) and quantification of spine survival after 7 days. (C) Long-term survival analysis in experiments where LTP was induced 24 h after LTD. Below: Maximum intensity projections of mCerulean fluorescence in dendritic segment harboring a responding spine that was successfully depressed on day 0 and potentiated on day 1 (yellow arrowhead). (D) Assessment

of synaptic weight changes induced by oLFS on day 0 and oTFS on day 1. Dashed box in left graph indicates all experiments where LTD was successfully induced on day 0. Only these spines were considered in the LTP experiment on day 1 (middle). Yellow shaded box indicates all experiments where LTP was successfully induced on day 1 (after LTD on day 0; LTD ► LTP). Red shaded box indicates experiments where oTFS did not lead to LTP (only LTD). Pie charts show quantification of spine survival after 7 days for these two conditions.

Fig. 5. The most recent plasticity event fully accounts for synaptic tenacity. (A) Long-term survival analysis of experiments where LTD was induced 24 h after LTP. Maximum intensity projections of mCerulean fluorescence in dendritic segment harboring a responding spine that was successfully potentiated on day 0 and depressed on day 1 (yellow arrowhead). (B) Assessment of synaptic weight changes induced by oTFS on day 0 and oLFS on day 1. Dashed box in left graph indicates all experiments where LTP was successfully induced on day 0. Only these spines were considered in the LTD experiment on day 1 (middle). Yellow shaded box indicates all experiments where LTD was successfully induced on day 1 (after LTP on day 0, LTP ► LTD). Note the low probability of depression after potentiation. Green shaded box encompasses experiments where oLFS did not lead to LTD or even led to LTP (only LTP). Pie charts show quantification of spine survival after 7 days for these two conditions. (C) Comparison of spine survival 7 days after various plasticity paradigms. Stimulated spines are shown as open circles; non-stimulated neighbors within 10 µm are shown as filled circles. Values for “control” and “LTD” are from Wiegert *et al*., 2013. (D) LTP stabilizes the spine carrying the potentiated synapse, but reduces the average lifetime of more distant (> 5 µm) spines on the same dendrite.

References

1. Chaudhuri R, Fiete I (2016) Computational principles of memory. *Nat Neurosci* 19(3):394–403.

2. Bliss T V, Lomo T (1973) Long-lasting potentiation of synaptic transmission in the dentate area of the anaesthetized rabbit following stimulation of the perforant path. *J Physiol* 232(2):331–356.

3. Holtmaat A, Caroni P (2016) Functional and structural underpinnings of neuronal assembly formation in learning. *Nat Neurosci* 19(12):1553–1562.

4. Berry KP, Nedivi E (2017) Spine Dynamics: Are They All the Same? *Neuron* 96(1):43–55.

5. Nagerl U V, Eberhorn N, Cambridge SB, Bonhoeffer T (2004) Bidirectional activity-dependent morphological plasticity in hippocampal neurons. *Neuron* 44(5):759–767.

6. Wiegert JS, Oertner TG (2013) Long-term depression triggers the selective elimination of weakly integrated synapses. *Proc Natl Acad Sci U S A* 110(47):E4510-9.

7. Bastrikova N, Gardner GA, Reece JM, Jeromin A, Dudek SM (2008) Synapse elimination accompanies functional plasticity in hippocampal neurons. *Proc Natl Acad Sci U S A* 105(8):3123–7.

8. De Roo M, Klauser P, Mendez P, Poglia L, Muller D (2008) Activity-dependent PSD formation and stabilization of newly formed spines in hippocampal slice cultures. *Cereb Cortex* 18(1):151–161.

9. Hill TC, Zito K (2013) LTP-induced long-term stabilization of individual nascent dendritic spines. *J Neurosci* 33(2):678–86.

10. Fujii S, Saito K, Miyakawa H, Ito K, Kato H (1991) Reversal of long-term potentiation (depotentiation) induced by tetanus stimulation of the input to CA1 neurons of guinea pig hippocampal slices. *Brain Res* 555(1):112–22.

11. Abraham WC, Huggett A (1997) Induction and reversal of long-term potentiation by repeated high-frequency stimulation in rat hippocampal slices. *Hippocampus* 7(2):137–

45.

12. O'Dell TJ, Kandel ER (1994) Low-frequency stimulation erases LTP through an NMDA receptor-mediated activation of protein phosphatases. *Learn Mem* 1(2):129–39.

13. Thomas MJ, Watabe AM, Moody TD, Makhinson M, O'Dell TJ (1998) Postsynaptic complex spike bursting enables the induction of LTP by theta frequency synaptic stimulation. *J Neurosci* 18(18):7118–26.

14. Berndt A, et al. (2011) High-efficiency channelrhodopsins for fast neuronal stimulation at low light levels. *Proc Natl Acad Sci U S A* 108(18):7595–600.

15. Moody TD, Thomas MJ, Makhinson M, O'Dell TJ (1998) 5-Hz stimulation of CA3 pyramidal cell axons induces a beta-adrenergic modulated potentiation at synapses on CA1, but not CA3, pyramidal cells. *Brain Res* 794(1):75–9.

16. Losonczy A, Magee JC (2006) Integrative properties of radial oblique dendrites in hippocampal CA1 pyramidal neurons. *Neuron* 50(2):291–307.

17. Attardo A, Fitzgerald JE, Schnitzer MJ (2015) Impermanence of dendritic spines in live adult CA1 hippocampus. *Nature* 523(7562):592–596.

18. Nishiyama J, Yasuda R (2015) Biochemical Computation for Spine Structural Plasticity. *Neuron* 87(1):63–75.

19. Mizuseki K, Buzsáki G (2013) Preconfigured, skewed distribution of firing rates in the hippocampus and entorhinal cortex. *Cell Rep* 4(5):1010–21.

20. Golding NL, Staff NP, Spruston N (2002) Dendritic spikes as a mechanism for cooperative long-term potentiation. *Nature* 418(6895):326–331.

21. Magee JC, Johnston D (1997) A synaptically controlled, associative signal for Hebbian plasticity in hippocampal neurons. *Science* 275(5297):209–213.

22. Grienberger C, Chen X, Konnerth A (2014) NMDA Receptor-Dependent Multidendrite Ca 2+ Spikes Required for Hippocampal Burst Firing In Vivo. *Neuron* 81(6):1274–1281.

23. Bittner KC, et al. (2015) Conjunctive input processing drives feature selectivity in hippocampal CA1 neurons. *Nat Neurosci* 18(8):1133–1142.

24. Sheffield MEJ, Adoff MD, Dombeck DA (2017) Increased Prevalence of Calcium Transients across the Dendritic Arbor during Place Field Formation. *Neuron* 96(2):490–504.e5.

25. Hasselmo ME, Bodelón C, Wyble BP (2002) A Proposed Function for Hippocampal Theta Rhythm: Separate Phases of Encoding and Retrieval Enhance Reversal of Prior Learning. *Neural Comput* 14(4):793–817.

26. Grunditz A, Holbro N, Tian L, Zuo Y, Oertner TG (2008) Spine neck plasticity controls postsynaptic calcium signals through electrical compartmentalization. *J Neurosci* 28(50):13457–13466.

27. Lu W, et al. (2001) Activation of synaptic NMDA receptors induces membrane insertion of new AMPA receptors and LTP in cultured hippocampal neurons. *Neuron* 29(1):243–254.

28. Shi SH, et al. (1999) Rapid spine delivery and redistribution of AMPA receptors after synaptic NMDA receptor activation. *Science* 284(5421):1811–1816.

29. Matsuzaki M, Honkura N, Ellis-Davies GC, Kasai H (2004) Structural basis of long-term potentiation in single dendritic spines. *Nature* 429(6993):761–766.

30. Körber N, Stein V (2016) In vivo imaging demonstrates dendritic spine stabilization by SynCAM 1. *Sci Rep* 6(1):24241.

31. Zeidan A, Ziv NE (2012) Neuroligin-1 Loss Is Associated with Reduced Tenacity of Excitatory Synapses. *PLoS One* 7(7):e42314.

32. Cane M, Maco B, Knott G, Holtmaat A (2014) The relationship between PSD-95 clustering and spine stability in vivo. *J Neurosci* 34(6):2075–86.

33. Kim H, Kunz PA, Mooney R, Philpot BD, Smith SL (2016) Maternal Loss of Ube3a Impairs Experience-Driven Dendritic Spine Maintenance in the Developing Visual Cortex. *J Neurosci* 36(17):4888–4894.

34. Bernardinelli Y, et al. (2014) Activity-Dependent Structural Plasticity of Perisynaptic Astrocytic Domains Promotes Excitatory Synapse Stability. *Curr Biol* 24(15):1679–1688.

35. Xu T, et al. (2009) Rapid formation and selective stabilization of synapses for enduring motor memories. *Nature* 462:915–919.

36. Yang G, Pan F, Gan W-B (2009) Stably maintained dendritic spines are associated with lifelong memories. *Nature* 462(7275):920–924.

37. Murakoshi H, Wang H, Yasuda R (2011) Local, persistent activation of Rho GTPases during plasticity of single dendritic spines. *Nature* 472(7341):100–104.

38. Yasuda R (2017) Biophysics of Biochemical Signaling in Dendritic Spines: Implications in Synaptic Plasticity. *Biophys J* 113(10):2152–2159.

39. Markram H, et al. (2015) Reconstruction and Simulation of Neocortical Microcircuitry. *Cell* 163(2):456–92.

40. Gee CE, Ohmert I, Wiegert JS, Oertner TG (2017) Preparation of Slice Cultures from Rodent Hippocampus. *Cold Spring Harb Protoc* 2017(2):pdb.prot094888.

41. Wiegert JS, Gee CE, Oertner TG (2017) Single-Cell Electroporation of Neurons. *Cold Spring Harb Protoc* 2017(2):pdb.prot094904.

42. Pologruto TA, Sabatini BL, Svoboda K (2003) ScanImage: Flexible software for operating laser scanning microscopes. *Biomed Eng Online* 2(1):13.

Figure 1

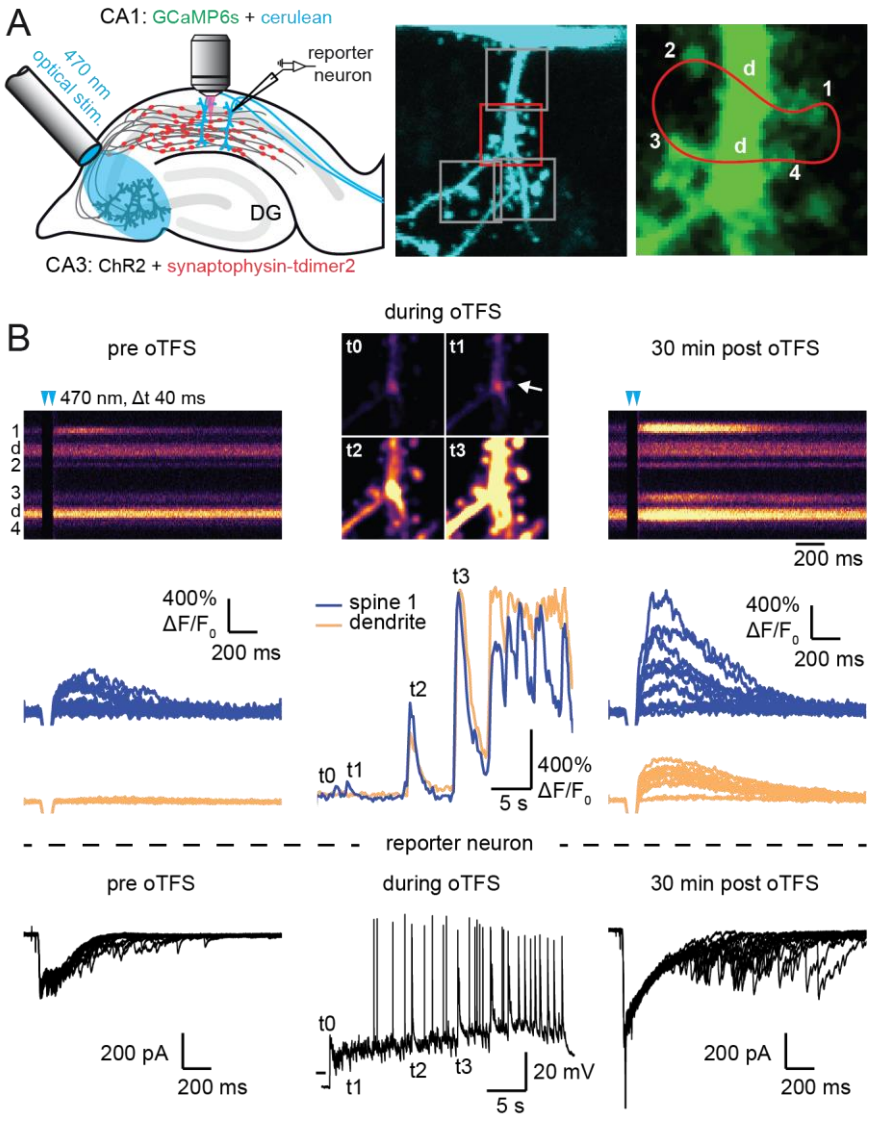

Figure 2

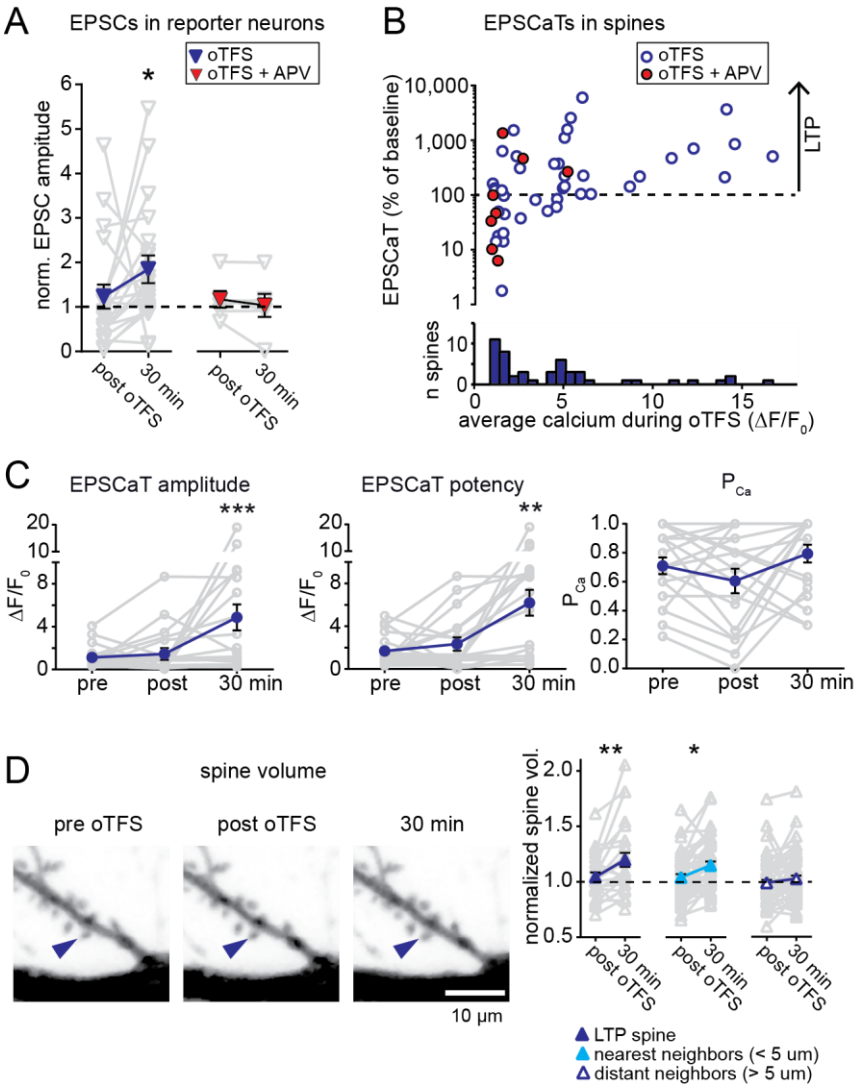

Figure 3

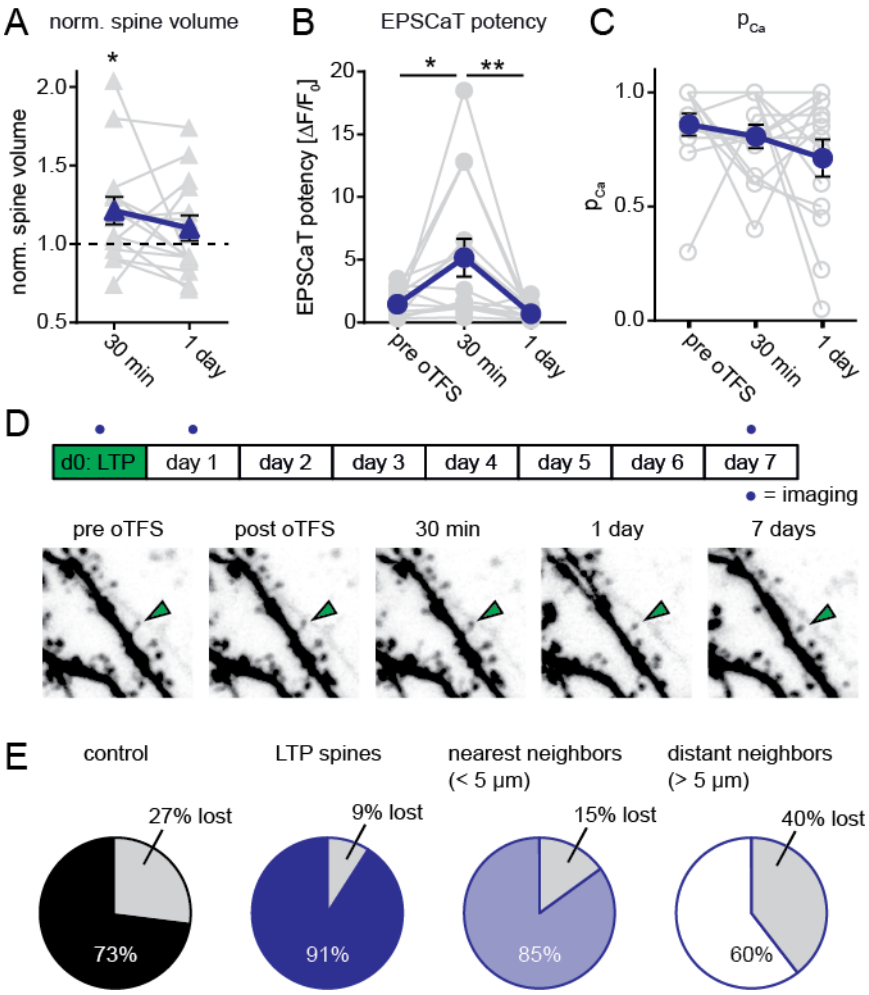

Figure 4

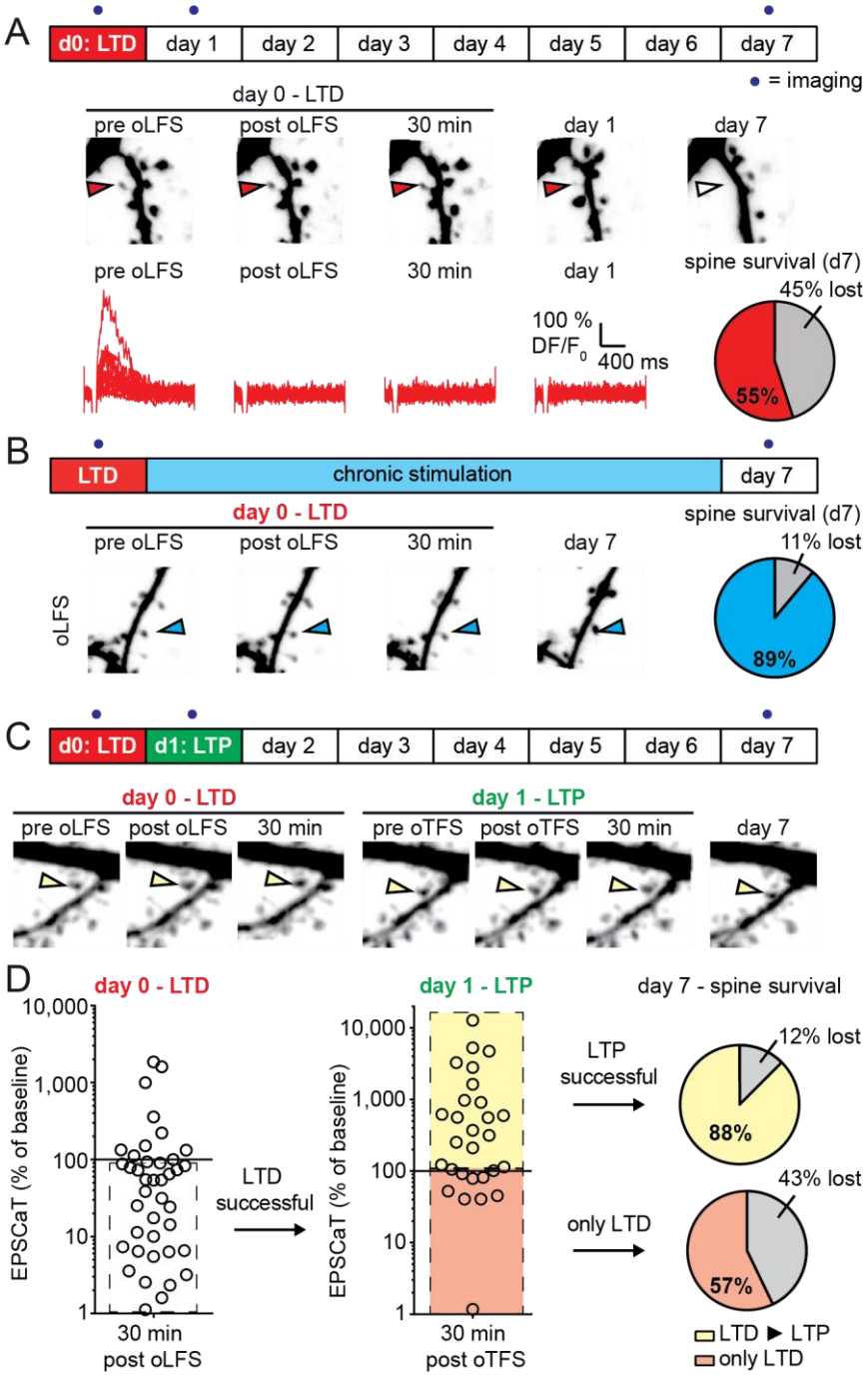

Figure 5

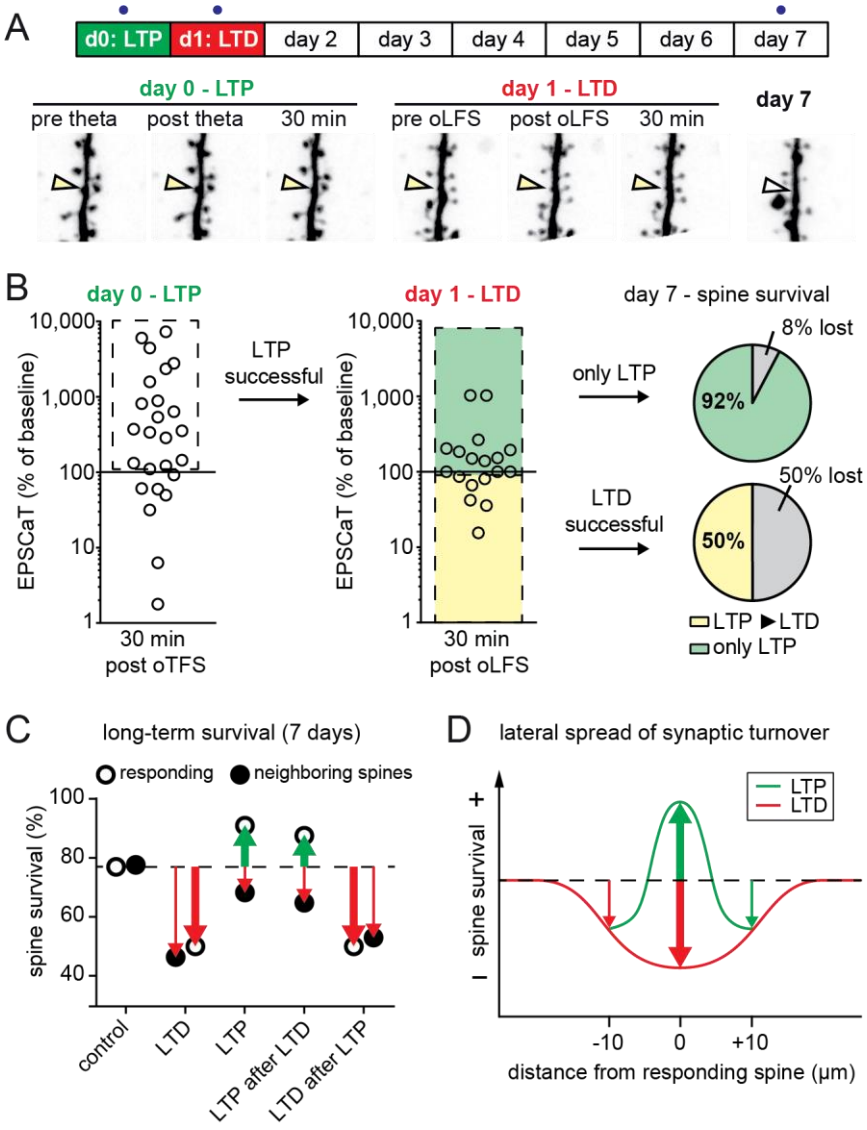

Supplemental figures

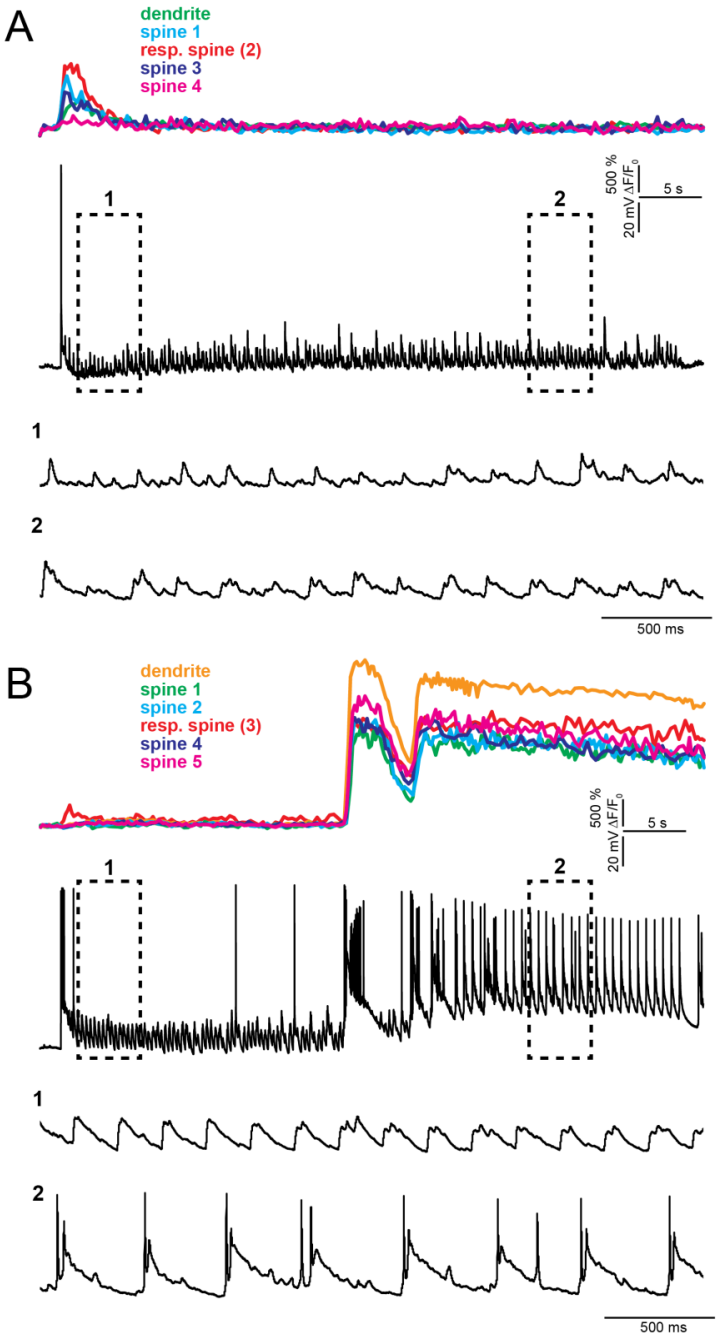

Fig. S1. Examples of optogenetic TFS experiments. (*A*) Experiment where no dendritic calcium spikes were observed in the GCaMP6s-expressing CA1 pyramidal cell (colored traces, top) and no complex spike bursts (CSBs) were triggered in the neighboring 'reporter' neuron (black traces). (*B*) Experiment with dendritic calcium spikes and synchronous CSBs in the reporter neuron.

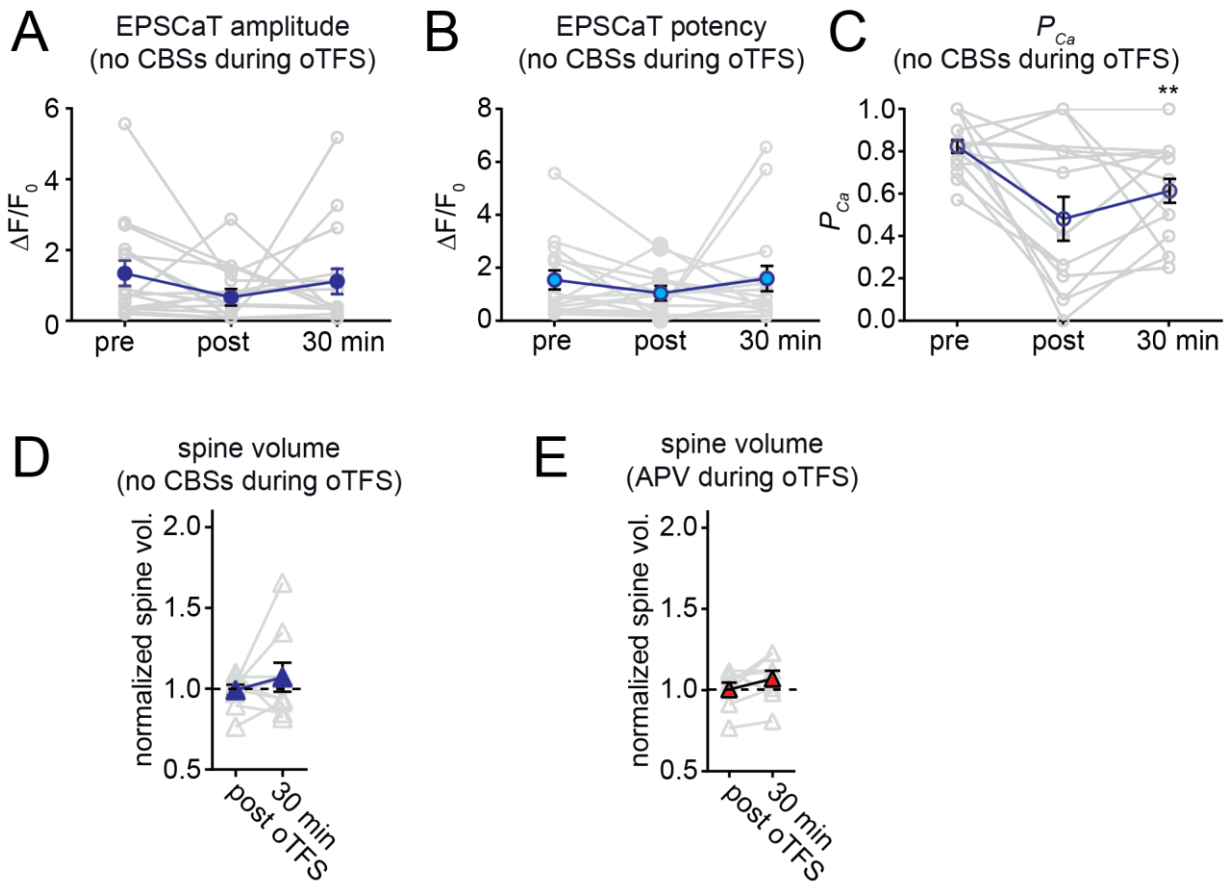

Fig. S2. Analysis of oTFS experiments where no dendritic calcium spikes were observed during the induction protocol.

(*A*) The null hypothesis, no change in EPSCaT amplitude after oTFS, could not be rejected ($p > 0.05$).

(*B*) The null hypothesis, no change in EPSCaT potency after oTFS, could not be rejected ($p > 0.05$).

(*C*) The probability of EPSCaTs was significantly reduced after oTFS ($p = 0.0098$). (A) – (C): nonparametric Friedman test followed by Dunn's multiple comparison test.

(*D*) The null hypothesis, no change in spine head volume after oTFS, could not be rejected ($p > 0.05$, Wilcoxon matched-pairs signed rank test).

(*E*) Analysis of all oTFS experiments where NMDA receptors were blocked during induction (APV). The null hypothesis, not change in spine head volume after oTFS, could not be rejected ($p > 0.05$, paired, two-tailed t-test).